

Article

# Impact of Chirp in High-Capacity Optical Metro Networks Employing Directly-Modulated VCSELs

Mariangela Rapisarda <sup>1</sup>, Alberto Gatto <sup>1</sup>, Paolo Martelli <sup>1</sup>, Paola Parolari <sup>1</sup>, Christian Neumeyr <sup>2</sup>, Michela Svaluto Moreolo <sup>3</sup>, Josep M. Fabrega <sup>3</sup>, Laia Nadal <sup>3</sup> and Pierpaolo Boffi <sup>1,\*</sup>

<sup>1</sup> Dip. Elettronica, Informazione e Bioingegneria, Politecnico di Milano, Piazza Leonardo da Vinci 32, 20133 Milano, Italy; mariangela.rapisarda@polimi.it (M.R.); alberto.gatto@polimi.it (A.G.); paolo.martelli@polimi.it (P.M.); paola.parolari@polimi.it (P.P.)

<sup>2</sup> Vertilas GmbH, Daimlerstr. 11d, D-85748 Garching, Germany; neumeyr@vertilas.com

<sup>3</sup> Centre Tecnològic de Telecomunicacions de Catalunya (CTTC/CERCA), Av. C. F. Gauss 7, 08860 Castelldefels, Barcelona, Spain; michela.svaluto@cttc.es (M.S.M.); jmfabrega@cttc.es (J.M.F.); laia.nadal@cttc.es (L.N.)

\* Correspondence: pierpaolo.boffi@polimi.it; Tel.: +39-02-23998923

Received: 31 October 2018; Accepted: 23 November 2018; Published: 27 November 2018



**Abstract:** Directly modulated long-wavelength vertical cavity surface emitting lasers (VCSELs) are considered for the implementation of sliceable bandwidth/bitrate variable transceivers for very high capacity transmission (higher than 50 Gb/s per wavelength) in metropolitan area systems characterized by reduced cost, power consumption, and footprint. The impact of the frequency chirp measured for InP VCSELs with different kinds of design (high-bandwidth very short cavity and widely-tunable with micro electro-mechanical systems (MEMS) top mirror) is analyzed in case of discrete multitone (DMT) direct modulation in combination with 25-GHz wavelength selective switch (WSS) filtering. The maximum transmitted capacity for both dual side- and single side-band DMT modulation is evaluated as a function of the number of crossed nodes in a mesh metro network, comparing VCSEL based transmitters performance also with the case of external electro-absorption modulator use. Finally, the maximum reach achieved based on the received optical signal to noise ratio (OSNR) and the fiber span length is discussed. The results confirm the possibility to use directly-modulated long-wavelength VCSELs for the realization of sliceable bandwidth/bitrate variable transmitters targeting 50-Gb/s capacity per polarization, also in the presence of 5 crossed WSSs for reaches of hundreds of kilometers in multi-span Erbium-doped fiber amplified (EDFA) metro links supported by coherent detection.

**Keywords:** direct modulation; discrete multitone; metro networks; optical communications; vertical cavity surface emitting lasers

## 1. Introduction

In recent years, we have witnessed continuous growth of bandwidth demand in the access and metropolitan area networks (MANs), as traffic remains almost confined to where it was generated. MANs must therefore evolve toward more efficient and agile architectures which are able to address multi-Tb/s transmission and routing over variable distances and topologies, supporting any kind of services such as 5G, Mobile Edge Computing, ultra-high density TV, etc. [1]. Moreover, other challenges should be faced, enabling a “pay-as-you-grow” scheme according to traffic scaling, minimizing the operational expenditures (OpEx) by achieving low footprint and low power consumption. The current transmission devices for metro network are evolving from the traditional approach by proposing

enhanced modulation schemes or, as an alternative, coherent transmission solutions, which today are used mainly for long haul transmission, and are characterized by high cost and high-power consumption. With these approaches, the expected performance enhancement in terms of throughput is limited to a factor  $\times 2$ – $\times 4$ , which seems to be inadequate to support 5G-and-beyond network requirements. Moreover, a migration towards more flexible, efficient, and agile paradigms is expected, owing to the aggregation of the metro/access networks, and for the support of heterogeneous networks.

Alternative energy- and cost-efficient photonic solutions can be effectively used, starting from the adoption of direct modulation (DM) of the laser sources; in particular, vertical cavity surface emitting lasers (VCSELs) allow a reduction of transmitter cost, power consumption, and footprint. Recently, a sliceable bandwidth/bitrate variable transceiver (S-BVT) based on VCSEL has been proposed for MAN applications [2]. In order to obtain high transmission capacities, long-wavelength InP VCSELs emitting in the C band can be directly modulated by multicarrier formats, such as discrete multitone (DMT) format, as demonstrated for reaches of a few tens of kms with direct detection (DD) [3,4], and for longer reach by DD and single sideband (SSB) modulation [2]. Thanks to bit and power loading at the digital signal processing (DSP) level, DMT is capable of addressing the efficient usage of the bandwidth resource as a function of the requested capacity and transmission distance, and allowing dynamic and flexible adaptation to traffic/channel conditions and spectrum fragmentation mitigation in MANs [5].

Multi-Tb/s transmitters can be obtained by aggregating multiple DM-VCSELs emitting in the C-band with dense wavelength division multiplexers in SOI chips [6,7] providing a fine granularity, e.g., 25 GHz. When the VCSEL is DM to obtain high capacities, the generated frequency chirp impacts significantly on the propagation performance [8], playing an important role, especially if the multiplexer filter bandwidths are comparable with the electrical signal bandwidth, and potentially limiting the VCSEL employment in high-capacity MAN applications.

In this paper, long-wavelength VCSEL sources are employed to realize multi-Tb/s transceivers for MAN applications; in particular, we focus the analysis on VCSEL sources emitting in the C-band, taking into account realistic optical sources and network filters. In the following sections, we analyze the impact of the frequency chirp induced by DM VCSELs when DMT is used to provide a rate higher than 50 Gb/s per wavelength. We take into account both dual side-band (DSB) and single side-band (SSB) DMT modulation while maintaining the modulated optical spectrum confined to 25-GHz spacing to guarantee very dense wavelength-division multiplexing (WDM) transmission. At the receiver side, in order to be able to bridge typical MAN distances, coherent detection (COH-D) is employed, which allows chromatic dispersion (CD) compensation by DSP post-processing.

In Section 2 chirp experimental measurements performed on two different kinds of InP long-wavelength VCSELs are presented. In Section 3 the performance for the two measured VCSELs chirp are compared; simulations of transmission employing DMT DM VCSELs and COH-D demonstrate reach distances of hundreds of kms typical of MANs. The considered OSNR are typical of MAN applications, ranging from 30 to 40 dB, which are able to support hundreds-kms-long SSMF propagations. Moreover, the impact of wavelength selective switching (WSS) filtering is evaluated as a function of the number of network nodes crossed in the MAN path and of the amount of chirp. Final discussions are presented in Section 4, concluding the paper.

## 2. Chirp Measurements

CD leads to a different phase accumulation for each spectral component of a modulated optical signal after fiber propagation. Thanks to coherent detection, the CD cumulated on the whole transmission path can be totally compensated for by DSP, removing the distortion on the signal and avoiding significant limitations to the transported capacity, as otherwise appears in case of DD [9]. Anyway, the distortion of the received electrical spectrum due to cumulated CD can be exploited to characterize the employed optical source in terms of chirp parameters. Owing to the double-sideband spectrum achieved by DM of the laser, destructive beating may occur at specific frequencies after the

DD process, resulting in a frequency-selective channel that could induce significant distortions on the signal spectrum. The frequency of the fading dips depends on the cumulated CD, moving towards lower frequencies for higher dispersion. Moreover, laser chirp parameters have a strong impact on the shape of the frequency-selective channel, modifying the position and the extent of the spectrum dips [10]. Therefore, a complete characterization of the optical source in terms of chirp properties can be achieved by fitting the uncompensated channel transfer function.

The interaction between phase and intensity modulation in a directly-modulated laser is described using the relation between the instantaneous frequency deviation  $\Delta\nu(t)$  and the optical modulated power  $P(t)$  [11]:

$$\Delta\nu(t) = \frac{\alpha}{4\pi} \left( \frac{1}{P(t)} \frac{\partial P(t)}{\partial t} + \kappa P(t) \right), \quad (1)$$

where  $\alpha$  is the linewidth enhancement factor and  $\kappa$  is the laser-specific adiabatic constant related to thermal effects, which depends on several laser parameters such as its gain saturation, carrier lifetime and confinement factor. The first term of Equation (1), which mainly depends on the  $\alpha$  factor, is the transient component, while the second one is the adiabatic chirp, which depends on the  $\kappa$  factor. A small-signal frequency response analysis can be used for modeling the optical source and obtain its specific chirp coefficients [12]. For a directly-modulated laser (DML), the general channel transfer function can be expressed as [10]:

$$H(\omega) = \left| \cos(\theta) - \sin(\theta) \alpha \left( 1 - j \frac{\omega_c}{\omega} \right) \right|, \quad (2)$$

where

$$\theta = \frac{LD\lambda_0^2\omega^2}{4\pi c}, \quad \omega_c = \kappa P_0, \quad (3)$$

and  $L$  is the fiber length,  $D$  the dispersion coefficient,  $\lambda_0$  the wavelength of the CW source,  $c$  the speed of light and  $P_0$  the mean optical power. The position of the frequency dips and the height of the secondary lobes are determined by an interplay of  $\alpha$  and  $D$ , while the extent of the dips (in particular of the first one) is primarily due to  $\omega_c$ , i.e., to the adiabatic component of the chirp.

This analysis technique has been used for measuring the chirp parameters of two different devices: the first is a 20-GHz long-wavelength VCSEL emitting at 1533.4 nm [13], while the second is an 8-GHz VCSEL tunable over about 70 nm in the third fiber window [14]. The former device is based on a short-cavity design, while the latter exploits a micro electro-mechanical systems (MEMS) top-mirror to achieve its very wide tunability. The two devices show different chirp performance owing to their specific technology.

The experimental setup exploited for VCSEL chirp parameter estimation is shown in Figure 1. In particular, the long-wavelength VCSEL is directly modulated by a vector network analyzer with 40-GHz bandwidth, which generates the RF signal to perform the small-signal modulation analysis. The VCSEL bias is 9 mA and 16 mA for the fixed and tunable devices, emitting around 2.5 mW and 0.9 mW, respectively. In case of the tunable VCSEL, the MEMS bias is fixed to 20 mA, while the temperature is maintained at 25 °C by a standard temperature controller. The optical signal then propagates in a standard single-mode fiber (SSMF) coil, and is received by an EDFA preamplifier followed by a p-intrinsic-n (PIN) photodiode with 25-GHz electrical bandwidth; a variable optical attenuator (VOA) performs the measurements at constant received power. The SSMF length ranges from 10 km to 34 km in order to change the cumulated CD at the receiver end.

At first, the optical back-to-back contribution featuring the spectral distortions due to the electro/optic (E/O) and opto/electronic (O/E) processes is measured and excluded in order to measure only the fiber power transfer function (i.e., removing the VCSEL and receiver transfer functions). Equation (2) is used to fit the obtained curves; the measured (continuous curves) and theoretical (dashed curves) frequency responses for the tunable and short-cavity VCSEL sources are shown in Figure 2a,b on 10-GHz and 25-GHz ranges, respectively. The different frequency ranges have been chosen owing to

the different E/O bandwidths. As expected, when the accumulated dispersion increases, the frequency dips move towards lower frequencies, reducing the electrical spectrum undistorted region. However, a difference in the position and the depth of the first frequency dip for the two lasers clearly appears, confirming the different chirp regime of the two devices. The tunable VCSEL, in fact, is mainly limited by the transient chirp, while the short-cavity device shows even a significant adiabatic chirp, as visible by the limited extent of the first frequency dip, which almost disappears for 24-km and 34-km SSMF channel transfer functions. The theoretical curves after fitting (dashed lines in Figure 2) show a good agreement with the experimental measurements, allowing a reliable estimation of VCSEL chirp parameters in both cases, reported in Table 1. The short-cavity VCSEL shows higher  $\alpha$  and  $\kappa$  factors, as expected from the device design based on a short-cavity technology. This laser design is capable of achieving wide modulation bandwidth, but a strong frequency chirp is induced during direct modulation, limiting its effectiveness in the presence of network nodes with narrow channel bandwidth.

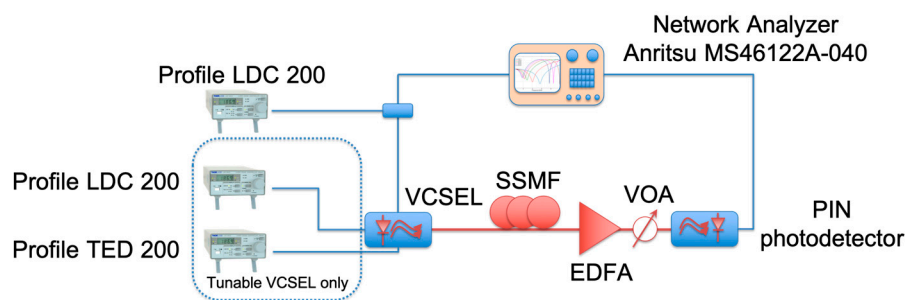


Figure 1. Experimental setup for chirp parameters measurement.

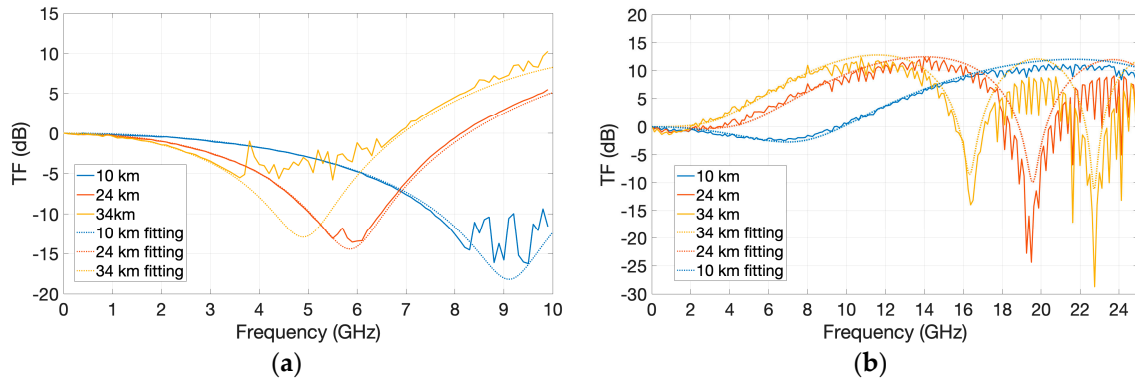


Figure 2. Channel transfer functions obtained after 10-km (blue), 24-km (red) and 34-km (yellow) SSMF propagation for: (a) 8-GHz tunable VCSEL and (b) 20-GHz short-cavity VCSEL.

Table 1. Measured chirp parameters of the two VCSEL sources.

Optical Source	$\alpha$	$\kappa$
Tunable VCSEL	2.75	$8.3 \times 10^{12}$
Short-cavity VCSEL	3.7	$1.52 \times 10^{13}$

### 3. Simulations

As previously demonstrated, InP long-wavelength VCSELs can show different amount of chirp, depending on their design and fabrication. When analyzing the transmission performance of DM-VCSELs this parameter plays a critical role especially in the presence of filtering associated to wavelength multiplexers and demultiplexers present inside the WDM MAN, e.g., at the network nodes. It should be noted that the chirp interplay with CD can be neglected in case of COH-D exploitation,

where CD DSP compensation can be easily performed. Moreover, as DM is exploited, the transmitted signal is just intensity modulated, and a simplified coherent receiver can be used [15]: after I and Q components recovery and CD compensation the I and Q square moduli are performed and summed up in order to obtain the originally transmitted intensity signal. This approach avoids the use of phase and frequency recovery, reducing the complexity of the receiver DSP and also relaxing the constraints on VCSEL and local oscillator (LO) linewidths. As a drawback, this operation cancels the advantages in terms of bit error rate (BER) as a function of signal to noise ratio (SNR) of COH-D.

Our simulations are obtained developing a modeling tool based on Matlab™ which includes all the transmitter, propagation, and receiver blocks. Specifically, the COH receiver exploits a 10-dBm per polarization LO with 100-kHz linewidth and has 25-GHz electrical bandwidth. The DM VCSEL is modeled considering both the intrinsic modulation properties and the extrinsic device parasitic components. The overall electrical modulation frequency response can be described by [16]:

$$H(f) = H_{int}(f) \cdot H_{par}(f) = const \cdot \frac{f_R^2}{f_R^2 + j\frac{\gamma}{2\pi}f - f^2} \cdot \frac{1}{1 + j\frac{f}{f_p}}, \quad (4)$$

where  $f_R$  is the relaxation resonance frequency,  $\gamma$  is the intrinsic damping factor and  $f_p$  is the parasitic cut-off frequency.

The simulations have been performed for three different chirp conditions, corresponding to the following three cases:

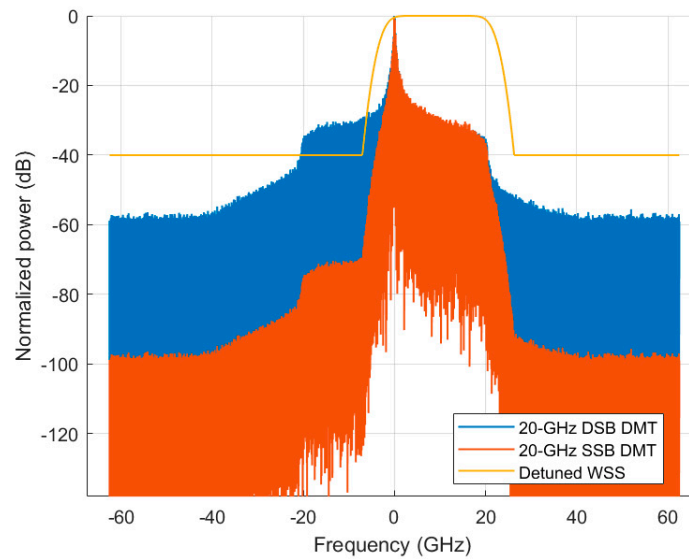
1. a directly-modulated VCSEL with chirp parameters as the short-cavity device
2. a directly-modulated VCSEL with chirp parameters as the tunable device
3. a CW 500-kHz laser followed by an electro-absorption modulator (EAM) with  $\alpha = 0.4$

For all the three cases, following [16] and Equation (4), the modulation frequency bandwidth is set to 18 GHz, although this bandwidth is now achieved only by the actual short-cavity devices. The VCSEL linewidth is 5 MHz, which is a suitable value for both long-wavelength VCSELs. The bias currents are set to 8 mA and 16 mA for case (1) and (2), respectively, while their modulation amplitudes are 8.5 mA and 26 mA respectively; thanks to the reduced amount of chirp, in fact, in the tunable VCSEL case, it is possible to exploit a higher modulation depth, allowing higher SNRs. The bias current and the modulation depth for case (3) are optimized in order to achieve an equivalent extinction ratio of 15 dB.

The impact of optical filtering is evaluated using the transfer function of a 25-GHz channel spacing WSS, which shows a 21-GHz full width half maximum (FWHM) [9]. The propagation medium is a SSMF, with 0.25 dB/km attenuation and 17 ps/nm km dispersion at 1550 nm. Fiber spans of 35 km and 65 km are considered with the employment of Erbium-doped fiber amplifiers (EDFAs) with 6-dB noise figure (NF) to compensate for the transmission losses of each span.

The performance is evaluated in the case of DMT modulation signals, considering DSB and SSB transmissions; in both conditions, the generated optical spectra have to occupy less than 25 GHz in order to be transmitted through cascaded WSSs, guaranteeing 25-GHz WDM spacing for fine granularity. For this reason, we tested a DSB DMT signal composed by 256 sub-carriers in 10 GHz range, i.e., the sub-carrier spacing is 39.062 MHz; occupying an optical bandwidth of around 20 GHz; a cyclic prefix (CP) of about 2.1% of the symbol length is also added. On the other hand, the SSB transmission is performed by properly detuning the WSS with respect to the carrier of a DMT signal composed by 256 sub-carriers in 20 GHz range, i.e., the sub-carrier spacing is 78.125 MHz; again, a CP of about 2.1% of the symbol length is added. Figure 3 shows the spectrum of the SSB signal obtained detuning the WSS in order to select half of the 20-GHz DMT DSB spectrum, while preserving the optical carrier.

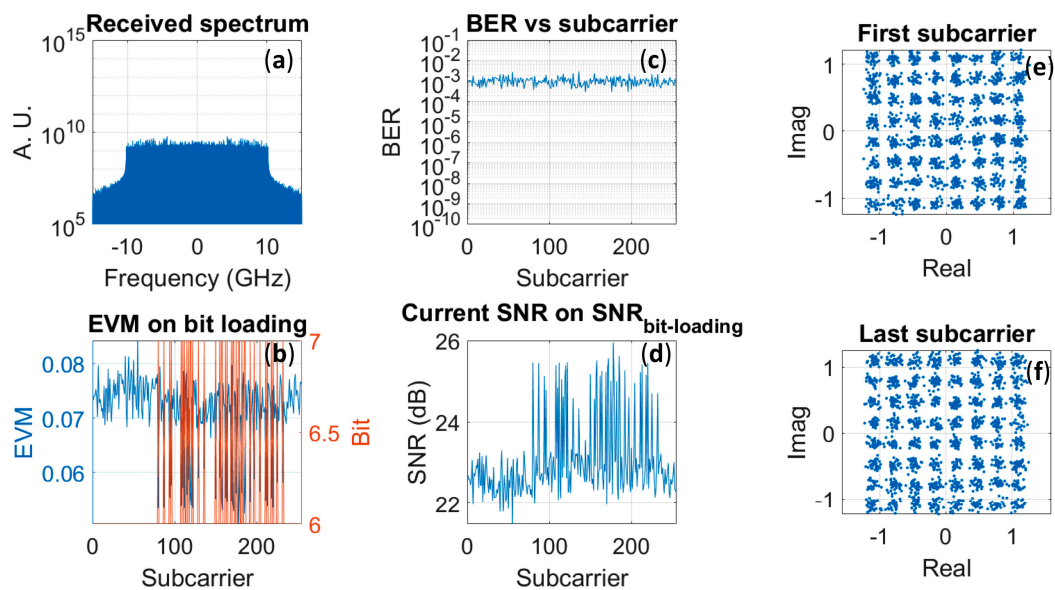




**Figure 3.** DMT SSB optical spectrum (red), obtained by a 9.5-GHz detuned WSS (orange) filtering of a DMT DSB signal with 20-GHz electrical bandwidth and 40-GHz optical bandwidth (blue).

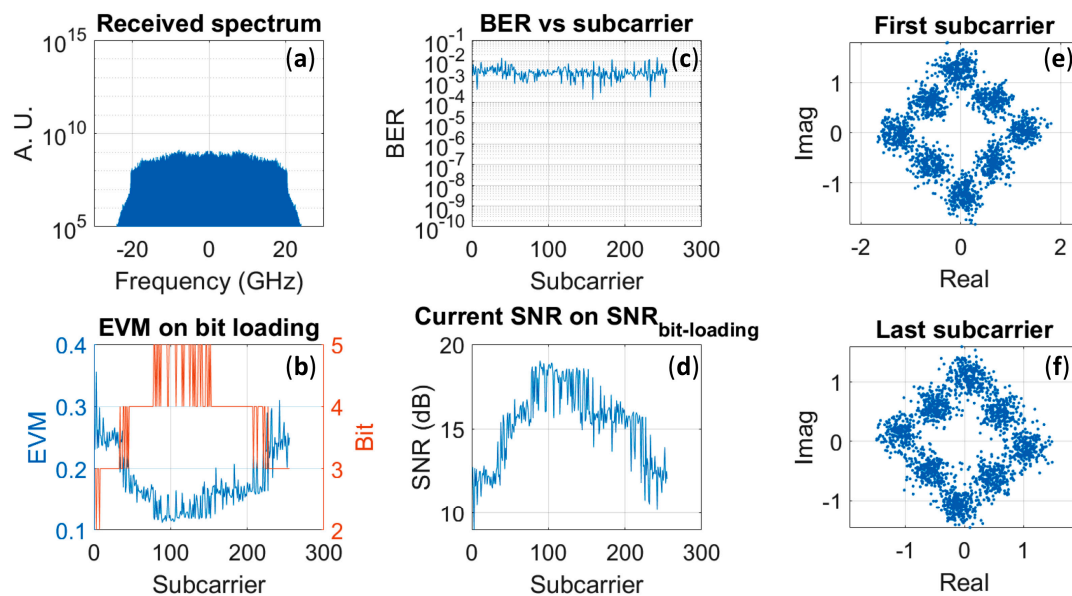
As can be seen, in order to mimic a realistic WSS transfer function with limited extinction, we imposed a maximum out-of-band attenuation of 40 dB. The left side of the optical spectrum is correctly filtered out, while a slight impact on the last subcarriers on the right appears due to the 21-GHz FWHM.

Together with CD compensation, the receiver DSP provides digital symbol synchronization, CP removal, sub-carriers phase recovery, demodulation, and error count. In the following section, the transmitted capacity is evaluated performing Chow’s bit loading algorithm [17] with a target BER of  $3.8 \times 10^{-3}$  (corresponding to 7% overhead hard decision FEC limit) for single-channel, single-polarization transmission. Figure 4a–f shows an example of the results obtained for DSB DMT modulation of the tunable VCSEL ( $\alpha = 2.75 \kappa = 8.3 \times 10^{12}$ ) in case of one WSS filtering and 40-dB OSNR. Figure 4a–f reports the received electrical spectrum, the bit loading, the BER per subcarrier and examples of received constellations.



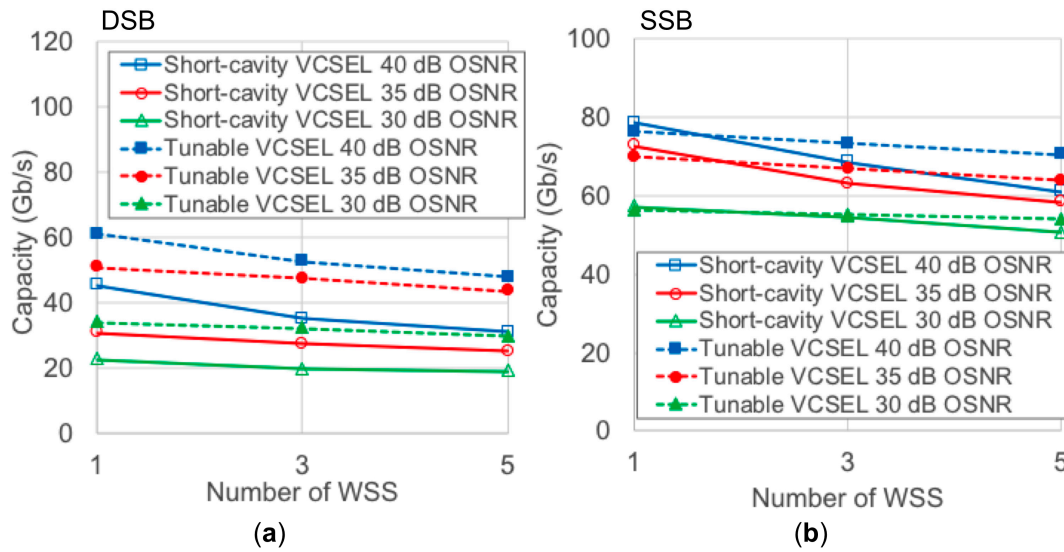
**Figure 4.** (a–f) Tunable VCSEL: DSB DMT (10 GHz) for single WSS filtering and 40-dB OSNR. (a) Received electrical spectrum; (b) Bit loading and corresponding EVM; (c) BER per subcarrier; (d) Bit-loading SNR; (e,f) Examples of received constellations.

Figure 5a–f reports the same graphs for the tunable VCSEL SSB DMT transmission in case of one WSS filtering and 40-dB OSNR for a WSS detuning of 9.5 GHz with respect to the VCSEL carrier. By comparing the received spectra, it is evident that SSB has a higher spectral efficiency, exploiting all the available VCSEL bandwidth and filling the whole 25-GHz channel bandwidth with the multicarrier signal. On the other hand, as expected, SSB suffers more of signal-signal beating interference (SSBI) [18] and of VCSEL and WSS bandwidth limitations: in fact, at low and high frequencies, SSB modulation presents lower SNRs with respect to the central frequencies (Figure 5d), and first and last subcarriers can support constellations with a lower level number, i.e., lower bit/symbol (Figure 5b,e,f. DSB modulation, instead, presents a flat SNR over all the subcarriers, supporting 6 or 7 bit per symbol per subcarrier; nevertheless, only half of the available E/O spectrum can be occupied in order to fit the 25-GHz optical spectrum constraint, limiting the maximum achievable capacity.



**Figure 5.** (a–f) Tunable VCSEL: SSB DMT for single WSS filtering (9.5-GHz detuned) and 40-dB OSNR. (a) Received electrical spectrum; (b) Bit loading and corresponding EVM; (c) BER per subcarrier; (d) Bit-loading SNR; (e,f) Examples of received constellations.

Figure 6 shows the capacities achieved for OSNR ranging from 30 dB to 40 dB in function of the number of crossed WSS in case of DSB DMT (Figure 6a) and in case of SSB DMT (Figure 6b). The results are reported for the two different chirp conditions considered so far. For comparison, also the transmission capacities are given for DSB and SSB DMT modulation in case of chirp typical of electro-absorption modulated lasers (EML), i.e.,  $\alpha = 0.4$ , are reported in Figure 7a,b respectively. As can be seen by comparing the dashed and continuous curves in Figure 6, the tunable VCSEL performance is better than the short-cavity VCSEL one, due to the lower chirp parameters. This is particularly true for DSB modulation, and is confirmed by Figure 7a, where the chirp of the EML is even lower. On the other hand, this is less evident for SSB modulation, where only for a higher number of crossed WSS the short-cavity VCSEL transported capacities are significantly lower than the tunable VCSEL ones, i.e., when chirp-filtering interaction is more detrimental. Moreover, by comparing Figures 6 and 7 it can be seen that, in case of lower OSNRs, a limited amount of chirp could be useful, since the performance of the EML are worse than the VCSELs. This effect could be due to the decrease of the carrier to signal power ratio (CSPR) in presence of chirp. CSPR has a strong impact on the capacity of DMT-modulated signal [19]; hence, its reduction due to chirp could mitigate the capacity decrease in the SSB condition.



**Figure 6.** Transmission capacities vs number of crossed WSS for: 40-dB OSNR (blue square), 35-dB OSNR (red circle), 30-dB OSNR (green triangle), and short-cavity VCSEL (continuous line open symbols), tunable VCSEL (dashed line full symbol) (a) DSB DMT modulation; (b) SSB DMT modulation.

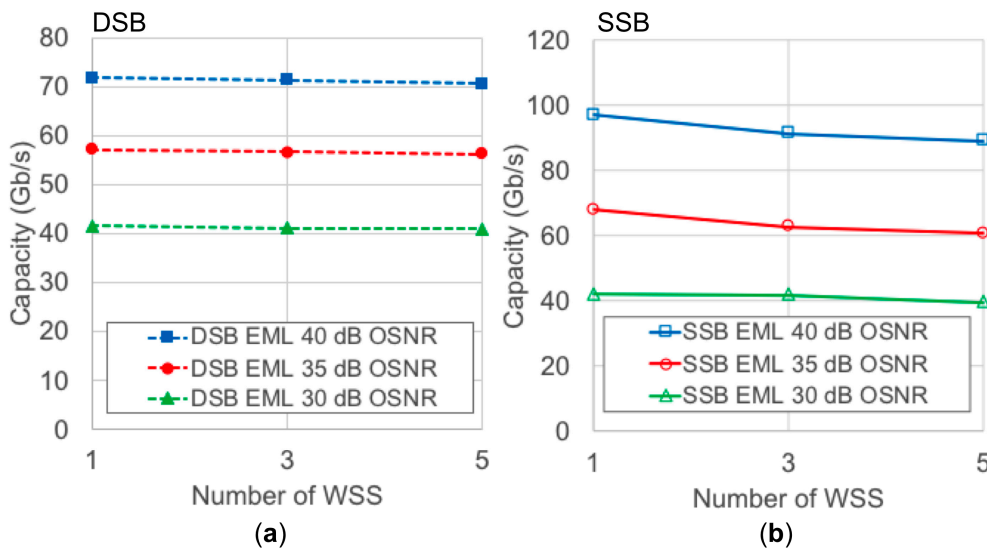


**Figure 7.** Transmission capacities vs number of crossed WSS for EML: 40-dB OSNR (blue square), 35-dB OSNR (red circle), 30-dB OSNR (green triangle). (a) DSB DMT modulation. (b) SSB DMT modulation.

Finally, Tables 2 and 3 summarize the transmitted capacities and SSMF reach as a function of the span length and of the number of crossed WSS respectively for DSB and SSB DMT modulations for the VCSEL based transmitters. The results are very encouraging for the exploitation of VCSELs in S-BVT transmitters targeting around 50 Gb/s capacity per polarization in presence of COH-D. In fact, especially for SSB DMT modulation also in presence of 5 WSS consecutive filtering, more than 50 Gb/s data rates are expected for OSNRs above 30 dB. This allows us to bridge more than 250 km SSMF when using EDFAs with typical NF performance and span length of 65 km; with shorter span length, even longer transmission distances can be supported, covering wider MANs. However, DMT DSB performance is heavily impaired by chirp and its interplay with filtering, limiting the achievable capacities to below 50 Gb/s also for 100-km transmission ranges.



**Table 2.** Transmitted capacities and SSMF reach for SSB DMT as a function of: span length, VCSEL type/chirp, and number of crossed WSS.

		OSNR	40 dB	35 dB	30 dB
Reach	35-km span		70 km	210 km	735 km
	65-km span		—	65 km	260 km
Short-cavity VCSEL	Capacity w 1 WSS		78.6 Gb/s	72.6 Gb/s	57.3 Gb/s
	Capacity w 3 WSS		68.6 Gb/s	63.1 Gb/s	54.5 Gb/s
	Capacity w 5 WSS		61 Gb/s	58.4 Gb/s	50.5 Gb/s
Tunable VCSEL	Capacity w 1 WSS		76.2 Gb/s	70 Gb/s	56.2 Gb/s
	Capacity w 3 WSS		73.3 Gb/s	67 Gb/s	55 Gb/s
	Capacity w 5 WSS		70.4 Gb/s	63.8 Gb/s	54 Gb/s

**Table 3.** Transmitted capacities and SSMF reach for DSB DMT as a function of: span length, VCSEL type/chirp, and number of crossed WSS.

		OSNR	40 dB	35 dB	30 dB
Reach	35-km span		70 km	210 km	735 km
	65-km span		—	65 km	260 km
Short-cavity VCSEL	Capacity w 1 WSS		45.5 Gb/s	30.9 Gb/s	22.8 Gb/s
	Capacity w 3 WSS		35.3 Gb/s	27.5 Gb/s	19.9 Gb/s
	Capacity w 5 WSS		31.1 Gb/s	25.2 Gb/s	19.2 Gb/s
Tunable VCSEL	Capacity w 1 WSS		61.2 Gb/s	51 Gb/s	34 Gb/s
	Capacity w 3 WSS		52.6 Gb/s	47.8 Gb/s	32.4 Gb/s
	Capacity w 5 WSS		48 Gb/s	43.75 Gb/s	30 Gb/s

#### 4. Discussion and Conclusions

We propose the use of directly-modulated long-wavelength VCSELs to implement S-BVT for capacity transmission higher than 50 Gb/s per wavelength in metropolitan area systems characterized by reduced cost, power consumption, and footprint. The most significant drawback of the direct modulation of VCSELs is frequency chirp, in particular when associated to optical filtering as in the network nodes. Thus, we analyzed its impact in case of dense WDM (25-GHz) WSS filtering in a DMT-based transmission system with direct modulation of the optical source and coherent detection at the receiver end to compensate for the cumulated chromatic dispersion. A performance evaluation by suitable simulations has been undertaken both in case of DSB and SSB transmissions. Since an optical bandwidth of 25 GHz can be filled up, a 10-GHz DSB and a 20-GHz SSB signals have been used. In order to obtain the chirp parameters to be used in reliable simulations for the transmission performance evaluation, preliminary measurements on InP VCSELs with two designs (a high-bandwidth device based on a short-cavity technology and a widely-tunable laser with MEMS top mirror) have been performed. A third case including the exploitation of an EML was added for reference; in order to focus on the chirp impact only, the remaining simulation parameters have been maintained unchanged for all the considered cases; in particular, the modulation bandwidth was set to 18 GHz. The maximum transmitted capacity for both DSB and SSB DMT modulation were evaluated as a function of the number of crossed nodes in a mesh metro network and of the received OSNR. The results indicate that, especially for many WSS crossings, in cases of DSB modulation, lower chirp parameters allow higher capacities, whereas in cases of SSB modulation and lower OSNR, the presence of a limited amount of chirp supports better performance, in particular for lower OSNR values (close to 30 dB). The presence of frequency chirp associated with direct modulation broadens the spectral occupancy in the optical domain. In cases of DSB transmission, the optical filter is perfectly centered on the VCSEL carrier, and the best results can be achieved by a chirp-free optical signal, which shows an optical spectrum with minimum bandwidth. On the other hand, in cases of SSB transmission, the frequency chirp superimposed on the signal permits to reduce the CSPR with respect to the

chirp-free condition, leading to an enhancement of the system performance. A trade-off between the amount of chirp and the SSB filter bandwidth to reach the optimal condition could be found, so further theoretical, simulative, and experimental analyses are ongoing. Transmitters hosting devices characterized by chirp parameters as the tunable VCSEL and exploiting 20-GHz SSB DMT modulation would thus support higher capacities; however, such a device is not currently available, since only the short-cavity technology is now able to guarantee modulation bandwidths higher than 10 GHz, which are needed to fully take advantage of the SSB spectral efficiency.

Finally, the maximum reach achieved according to the received OSNR and the fiber span length was discussed. The results confirm the possibility of using directly-modulated long-wavelength VCSELs for the realization of transmitters targeting 50-Gb/s capacity per polarization, also in presence of 5 crossed WSSs for reaches of hundreds of kilometers in multi-span EDFA-amplified metro links, supported by coherent detection.

The reported simulative analysis shows that the VCSEL-based optical communication system envisaged for metro area networks could represent a suitable solution to reach multi Tb/s capacities, simultaneously decreasing costs, footprint, and power consumption with respect to traditional approaches based on I/Q modulation and standard coherent detection. Moreover, the proposed architecture can be easily adapted to short-reach and datacenters scenarios using the O-band of the optical communications. In this wavelength range, thanks to the limited impact of chromatic dispersion, even direct detection could be a suitable option, further reducing the costs, footprint, power consumption, and complexity of the transmission system.

**Author Contributions:** Funding acquisition, P.B.; Investigation, A.G. and P.M.; Methodology, M.S.M., J.M.F. and L.N.; Resources, C.N.; Software, M.R.; Supervision, P.B.; Visualization, P.P.; Writing—original draft, M.R. and A.G.; Writing—review & editing, P.P., M.S.M., and P.B.

**Funding:** This paper is part of the PASSION project that has received funding from the European Union's Horizon 2020 research and innovation programme under grant agreement No. 780326.

**Acknowledgments:** The authors would like to thank Michele D'Amico and Gian Guido Gentili for lending the Vector Analyzer.

**Conflicts of Interest:** The authors declare no conflict of interest.

## References

1. Cisco Visual Networking Index: Forecast and Methodology, 2016–2021. Available online: <https://www.cisco.com/c/en/us/solutions/collateral/service-provider/visual-networking-index-vni/complete-white-paper-c11-481360.html> (accessed on 15 November 2018).
2. Svaluto Moreolo, M.; Nadal, L.; Fabrega, J.M.; Vilchez, F.J.; Casellas, R.; Muñoz, R.; Neumeyr, C.; Gatto, A.; Parolari, P.; Boffi, P. Modular SDN-enabled S-BVT Adopting Widely Tunable MEMS VCSEL for Flexible/Elastic Optical Metro Networks. In Proceedings of the OFC 2018, San Diego, CA, USA, 11–15 March 2018; p. M1A.7.
3. Xie, C.; Dong, P.; Randel, S.; Pileri, D.; Winzer, P.; Spiga, S.; Kögel, B.; Neumeyr, C.; Amann, M.-C. Single VCSEL 100-Gb/s Short-Reach System Using Discrete Multi-Tone Modulation and Direct Detection. In Proceedings of the OFC 2015, Los Angeles, CA, USA, 22–26 March 2018; p. Tu2H.2.
4. Gatto, A.; Parolari, P.; Neumeyr, C.; Boffi, P. Beyond 25 Gb/s Directly-Modulated Widely Tunable VCSEL for Next Generation Access Network. In Proceedings of the OFC 2018, San Diego, CA, USA, 11–15 March 2018; p. Th1E.2.
5. Svaluto Moreolo, M.; Fabrega, J.M.; Nadal, L.; Vilchez, F.J.; Mayoral, A.; Vilalta, R.; Muñoz, R.; Casellas, R.; Martinez, R.; Nishihara, M.; et al. SDN-Enabled Sliceable BVT Based on Multicarrier Technology for Multi-Flow Rate/Distance and Grid Adaptation. *J. Lightwave Technol.* **2016**, *34*, 1516–1522. [[CrossRef](#)]
6. Okamoto, K. Wavelength-division-multiplexing devices in thin SOI: Advances and prospects. *IEEE J. Sel. Top. Quantum Electron.* **2014**, *20*, 8200410. [[CrossRef](#)]
7. Malka, D.; Katz, G. An Eight-Channel C-Band Demux Based on Multicore Photonic Crystal Fiber. *Nanomaterials* **2018**, *8*, 845. [[CrossRef](#)] [[PubMed](#)]

8. Gatto, A.; Boletti, A.; Boffi, P.; Martinelli, M. Adjustable-chirp VCSEL-to-VCSEL injection locking for 10-Gb/s transmission at 1.55  $\mu\text{m}$ . *Opt. Express* **2009**, *17*, 21748–21753. [[CrossRef](#)] [[PubMed](#)]
9. Gatto, A.; Argenio, D.; Boffi, P. Very high-capacity short-reach VCSEL systems exploiting multicarrier intensity modulation and direct detection. *Opt. Express* **2016**, *24*, 12769–12775. [[CrossRef](#)] [[PubMed](#)]
10. Anet Neto, L.; Erasme, D.; Genay, N.; Chanclou, P.; Deniel, Q.; Traore, F.; Anfray, T.; Hmadou, R.; Aupetit-Berthelemot, C. Simple estimation of fiber dispersion and laser chirp parameters using the downhill simplex fitting algorithm. *J. Lightwave Technol.* **2013**, *31*, 334–342. [[CrossRef](#)]
11. Koch, T.L.; Bowers, J.E. Nature of wavelength chirping in directly modulated semiconductor lasers. *Electron. Lett.* **1984**, *20*, 1038–1040. [[CrossRef](#)]
12. Srinivasan, R.C.; Cartledge, J.C. On using fiber transfer functions to characterize laser chirp and fiber dispersion. *IEEE Photon. Technol. Lett.* **1995**, *7*, 1327–1329. [[CrossRef](#)]
13. Karinou, F.; Stojanovic, N.; Daly, A.; Neumejr, C.; Ortsiefer, M. 1.55- $\mu\text{m}$  long-wavelength VCSEL-based optical interconnects for short-reach networks. *J. Lightwave Technol.* **2016**, *34*, 2897–2904. [[CrossRef](#)]
14. Paul, S.; Gierl, C.; Cesar, J.; Le, Q.T.; Malekizandi, M.; Kogel, B.; Neumejr, C.; Ortsiefer, M.; Kuppers, F. 10-Gb/s direct modulation of widely tunable 1550-nm MEMS VCSEL. *IEEE J. Sel. Top. Quantum Electron.* **2015**, *21*, 1700908. [[CrossRef](#)]
15. Xie, C.; Spiga, S.; Dong, P.; Winzer, P.; Bergmann, M.; Kogel, B.; Neumejr, C.; Amann, M.-C. 400-Gb/s PDM-4PAM WDM system using a monolithic  $2 \times 4$  VCSEL array and coherent detection. *J. Lightwave Technol.* **2015**, *33*, 670–677. [[CrossRef](#)]
16. Pulikkaseril, C.; Stewart, L.A.; Roelens, M.A.F.; Baxter, G.W.; Poole, S.; Frisken, S. Spectral modeling of channel band shapes in wavelength selective switches. *Opt. Express* **2011**, *19*, 8458–8470. [[CrossRef](#)] [[PubMed](#)]
17. Chow, P.S.; Cioffi, J.M.; Bingham, J.A.C. A practical discrete multitone transceiver loading algorithm for data transmission over spectrally shaped channels. *IEEE Trans. Commun.* **1995**, *43*, 773–775. [[CrossRef](#)]
18. Lowery, A.J.; Armstrong, J. Orthogonal-frequency-division multiplexing for dispersion compensation of long-haul optical systems. *Opt. Express* **2006**, *14*, 2079–2084. [[CrossRef](#)] [[PubMed](#)]
19. Pilori, D.; Fludger, C.; Gaudino, R. Comparing DMT variants in medium-reach 100G optically amplified systems. *J. Lightwave Technol.* **2016**, *34*, 3389–3399. [[CrossRef](#)]



© 2018 by the authors. Licensee MDPI, Basel, Switzerland. This article is an open access article distributed under the terms and conditions of the Creative Commons Attribution (CC BY) license (<http://creativecommons.org/licenses/by/4.0/>).